Supporting Information for

Giant, magnet-free, and room-temperature Hall-like heat transfer

Liujun Xu[a,b,1], Jinrong Liu[c,1], Guoqiang Xu[a], Jiping Huang[c,2], and Cheng-Wei Qiu[a,2]

[a]Department of Electrical and Computer Engineering, National University of Singapore, Singapore 117583, Singapore. [b]Graduate School of China Academy of Engineering Physics, Beijing 100193, China. [c]Department of Physics, State Key Laboratory of Surface Physics, and Key Laboratory of Micro and Nano Photonic Structures (MOE), Fudan University, Shanghai 200438, China.

[1]Liujun Xu and Jinrong Liu contributed equally to this work.

[2]To whom correspondence may be addressed. Email: jphuang@fudan.edu.cn; chengwei.qiu@nus.edu.sg

This PDF file includes:

Supporting text
Figures S1 to S9
SI References

Supplementary Section 1: Basic properties of thermal chirality

Thermal chirality is reflected in a Hall thermal conductivity tensor $\overleftrightarrow{\kappa}$ with the form of

$$\overleftrightarrow{\kappa} = \begin{bmatrix} \kappa_{\mathrm{xx}} & \kappa_{\mathrm{yx}} \\ \kappa_{\mathrm{xy}} & \kappa_{\mathrm{yy}} \end{bmatrix}, \tag*{[S1]}$$

with $\kappa_{\mathrm{xx}} = \kappa_{\mathrm{yy}}$ and $\kappa_{\mathrm{xy}} = -\kappa_{\mathrm{yx}}$. We consider a rotation operation described by the rotation matrix S,

$$S = \begin{bmatrix} \cos\theta_0 & -\sin\theta_0 \\ \sin\theta_0 & \cos\theta_0 \end{bmatrix}, \tag*{[S2]}$$

where θ_0 is anticlockwise rotation angle. The thermal conductivity tensor $\overleftrightarrow{\kappa}'$ after rotation is

$$\overleftrightarrow{\kappa}' = \frac{S\overleftrightarrow{\kappa}S^{\dagger}}{\det S} = \begin{bmatrix} \kappa'_{\mathrm{xx}} & \kappa'_{\mathrm{yx}} \\ \kappa'_{\mathrm{xy}} & \kappa'_{\mathrm{yy}} \end{bmatrix}, \tag*{[S3]}$$

where the components take the form of

$$\kappa'_{\mathrm{xx}} = \kappa_{\mathrm{xx}}\cos^2\theta_0 + \kappa_{\mathrm{yy}}\sin^2\theta_0 - \left(\kappa_{\mathrm{xy}} + \kappa_{\mathrm{yx}}\right)\cos\theta_0\sin\theta_0, \tag*{[S4]}$$

$$\kappa'_{\mathrm{yy}} = \kappa_{\mathrm{yy}}\cos^2\theta_0 + \kappa_{\mathrm{xx}}\sin^2\theta_0 + \left(\kappa_{\mathrm{xy}} + \kappa_{\mathrm{yx}}\right)\cos\theta_0\sin\theta_0, \tag*{[S5]}$$

$$\kappa'_{\mathrm{xy}} = \kappa_{\mathrm{xy}}\cos^2\theta_0 - \kappa_{\mathrm{yx}}\sin^2\theta_0 + \left(\kappa_{\mathrm{xx}} - \kappa_{\mathrm{yy}}\right)\cos\theta_0\sin\theta_0, \tag*{[S6]}$$

$$\kappa'_{\mathrm{yx}} = \kappa_{\mathrm{yx}}\cos^2\theta_0 - \kappa_{\mathrm{xy}}\sin^2\theta_0 + \left(\kappa_{\mathrm{xx}} - \kappa_{\mathrm{yy}}\right)\cos\theta_0\sin\theta_0. \tag*{[S7]}$$

Due to $\kappa_{\mathrm{xx}} = \kappa_{\mathrm{yy}}$ and $\kappa_{\mathrm{xy}} = -\kappa_{\mathrm{yx}}$, Eqs. (S4)-(S7) can be simplified as

$$\kappa'_{\mathrm{xx}} = \kappa_{\mathrm{xx}}, \tag*{[S8]}$$

$$\kappa'_{\mathrm{yy}} = \kappa_{\mathrm{yy}}, \tag*{[S9]}$$

$$\kappa'_{\mathrm{xy}} = \kappa_{\mathrm{xy}}, \tag*{[S10]}$$

$$\kappa'_{\mathrm{yx}} = \kappa_{\mathrm{yx}}. \tag*{[S11]}$$

Any rotation operation does not change a Hall thermal conductivity tensor.

Since there is no real-number solution to $\kappa'_{\mathrm{xy}} = \kappa'_{\mathrm{yx}} = 0$, a Hall thermal conductivity tensor cannot be diagonalized in the real-number field. For proof, we suppose λ is the eigenvalue and solve the following equation,

$$|\overleftrightarrow{\kappa} - \lambda I| = 0, \tag*{[S12]}$$

where I is the unit matrix. Equation (S12) can be expanded as

$$\lambda^2 - \left(\kappa_{\mathrm{xx}} + \kappa_{\mathrm{yy}}\right)\lambda + \kappa_{\mathrm{xx}}\kappa_{\mathrm{yy}} - \kappa_{\mathrm{xy}}\kappa_{\mathrm{yx}} = 0. \tag*{[S13]}$$

We can further derive

$$\Delta = \left(\kappa_{\mathrm{xx}} - \kappa_{\mathrm{yy}}\right)^2 + 4\kappa_{\mathrm{xy}}\kappa_{\mathrm{yx}} = -4\kappa_{\mathrm{xy}}^2 < 0. \tag*{[S14]}$$

$\Delta < 0$ indicates no real-number solution to λ. If we solve the equation in the complex-number field, we can derive

$$\lambda_{\pm} = \frac{\kappa_{\mathrm{xx}} + \kappa_{\mathrm{yy}}}{2} \pm i\sqrt{-\kappa_{\mathrm{xy}}\kappa_{\mathrm{yx}}}. \tag*{[S15]}$$

We further explore the temperature and heat flux properties of thermal chirality by applying a longitudinal temperature gradient. The upper and lower boundaries are periodic, with continuous temperatures and heat fluxes. A transverse heat flux (the gray arrows in Fig. S1*A*) appears due to the nonzero off-diagonal components of a Hall thermal conductivity tensor. The periodic boundary conditions allow the transverse heat flux to flow out, so the temperature profile is the same as the case without thermal chirality, demonstrating a uniform longitudinal temperature gradient (Fig. S1*A*). The temperature and transverse heat flux profiles of an active thermal lattice are also presented in Fig. S1*B* and *C*. The artificial structure effectively has a Hall thermal conductivity, so thermal chirality appears definitely.

In contrast, anisotropy with $\kappa_{\mathrm{xy}} = \kappa_{\mathrm{yx}}$ distinctly differs from thermal chirality because a rotation operation changes the thermal conductivity tensor; see Eqs. (S4)-(S7). The temperature profile of anisotropy is identical to thermal chirality in a longitudinal temperature gradient, but the difference appears when using other boundary conditions like point heat sources. The temperature profiles of Hall (or anisotropic) thermal conductivities are presented in Fig. S2*A*-*C* (or Fig. S2*D*-*F*). Since thermal chirality breaks the space inversion symmetry, the mirror symmetry of temperature distributions is not maintained (Fig. S2*G*) even at symmetric positions (e.g., the blue dashed lines in Fig. S2*A*-*C*). However, anisotropy does not break the space inversion symmetry, so the temperature distributions at symmetric positions have mirror symmetry (Fig. S2*G*). Thus, thermal chirality inherently differs from anisotropy regarding rotation invariance and symmetry breaking.

Supplementary Section 2: Description of solid heat transfer

The governing equation of solid heat transfer in a unit cell containing a rotating particle is

$$\rho C\frac{\partial T}{\partial t}+\rho C v\nabla T-\kappa\nabla^2 T=Q, \qquad \text{[S16]}$$

where ρ is mass density, C is heat capacity, v is moving velocity, κ is thermal conductivity, and Q is heat power. For a steady and passive case, Eq. (S16) is reduced to

$$v\nabla T-D\nabla^2 T=0, \qquad \text{[S17]}$$

where $D=\kappa/(\rho C)$ is thermal diffusivity. We can expand Eq. (S17) in the cylindrical coordinates (r,θ) and derive $\nabla=\frac{\partial}{\partial r}\hat{r}+\frac{1}{r}\frac{\partial}{\partial\theta}\hat{\theta}$ and $\nabla^2=\frac{\partial^2}{\partial r^2}+\frac{1}{r}\frac{\partial}{\partial r}+\frac{1}{r^2}\frac{\partial^2}{\partial\theta^2}$, where $\hat{r}$ and $\hat{\theta}$ are the unit vectors. Equation (S17) can be rewritten as

$$\Omega\frac{\partial T}{\partial\theta}-D\left(\frac{\partial^2 T}{\partial r^2}+\frac{1}{r}\frac{\partial T}{\partial r}+\frac{1}{r^2}\frac{\partial^2 T}{\partial\theta^2}\right)=0, \qquad \text{[S18]}$$

where $\Omega=v/r$ is angular velocity.

The temperature profile $T_{\rm p}$ in the particle has the form of

$$T_{\rm p}=F(r)G(\theta), \qquad \text{[S19]}$$

where $F(r)$ and $G(\theta)$ are the radial and angular distribution functions. The substitution of Eq. (S19) into Eq. (S18) yields

$$\frac{1}{F}\left(r^2F''+rF'\right)=\frac{1}{G}\left(\frac{\Omega r^2}{D}G'-G''\right), \qquad \text{[S20]}$$

where the superscript denotes derivation. $G(\theta)$ is periodic regarding θ and can be expressed as $G(\theta)=e^{i\theta}$. Equation (S20) can be simplified as

$$r^2F''+rF'-\left(\frac{\Omega r^2}{D}i+1\right)F=0. \qquad \text{[S21]}$$

With a variable change $x=\sqrt{\Omega/D}r$, Eq. (S21) can be rewritten as

$$x^2f''+xf'-(x^2i+1)f=0. \qquad \text{[S22]}$$

The general solution to Eq. (S22) is the first-order Kelvin function (1-4),

$$f(x)=\mathrm{ber}(x)+i\mathrm{bei}(x). \qquad \text{[S23]}$$

Then we can derive

$$T_{\rm p}(r,\theta)=M\big(x(r)\big)\cos\Big(\theta-\phi\big(x(r)\big)\Big), \qquad \text{[S24]}$$

$$\frac{\partial T_{\rm p}(r,\theta)}{\partial r}=\sqrt{\frac{\Omega}{D}}M\big(x(r)\big)\cos\Big(\theta-\phi\big(x(r)\big)+\frac{\pi}{4}\Big), \qquad \text{[S25]}$$

where $M(x)$ is the magnitude of $f(x)$, and $\phi(x)$ reflects the rotation effect.

We use a stationary particle with an effective thermal conductivity $\kappa_{\rm p}^*$ to replace the rotating particle. The heat conduction equation without rotation becomes

$$\kappa\left(\frac{\partial^2 T}{\partial r^2}+\frac{1}{r}\frac{\partial T}{\partial r}+\frac{1}{r^2}\frac{\partial^2 T}{\partial\theta^2}\right)=0. \qquad \text{[S26]}$$

The general solution to Eq. (S26) is

$$T=T_0+\left(Ar+\frac{B}{r}\right)\cos\theta, \qquad \text{[S27]}$$

where T_0 is a reference temperature set as zero for brevity, and A and B are two constants. The temperature distributions in the matrix $T_{\rm m}$ and particle $T_{\rm p}^*$ are

$$T_{\rm m}=\left(A_{\rm m}r+\frac{B_{\rm m}}{r}\right)\cos\theta, \qquad \text{[S28]}$$

$$T_{\rm p}^*=A_{\rm p}^*r\cos\theta, \qquad \text{[S29]}$$

where $B_{\rm m}$ and $A_{\rm p}^*$ are two constants determined by the boundary conditions, and $A_{\rm m}$ is the applied temperature gradient. The continuities of temperatures and heat fluxes on the boundary are described by

$$T_{\rm m}(r=R)=T_{\rm p}^*(r=R), \qquad \text{[S30]}$$

$$-\kappa_{\mathrm{m}}\frac{\partial T_{\mathrm{m}}}{\partial r}(r=R)=-\kappa_{\mathrm{p}}^{*}\frac{\partial T_{\mathrm{p}}^{*}}{\partial r}(r=R), \tag{S31}$$

where κ_{m} is the thermal conductivity of the matrix, and R is the radius of the particle. Substituting Eqs. (S28) and (S29) into Eqs. (S30) and (S31), we can derive

$$A_{\mathrm{p}}^{*}=\frac{2\kappa_{\mathrm{m}}}{\kappa_{\mathrm{m}}+\kappa_{\mathrm{p}}^{*}}A_{\mathrm{m}}, \tag{S32}$$

$$B_{\mathrm{m}}=\frac{(\kappa_{\mathrm{m}}-\kappa_{\mathrm{p}}^{*})R^{2}}{\kappa_{\mathrm{m}}+\kappa_{\mathrm{p}}^{*}}A_{\mathrm{m}}. \tag{S33}$$

Generally, T_{p}^{*} is different from T_{p}, but we can find a specific condition to make their difference minimum. We define the difference as

$$\int_{0}^{2\pi}\left(T_{\mathrm{p}}(r=R)-T_{\mathrm{p}}^{*}(r=R)\right)^{2}d\theta, \tag{S34}$$

which can be rewritten as

$$\int_{0}^{2\pi}\left(M\big(x(R)\big)\cos\Big(\theta-\phi\big(x(R)\big)\Big)-\frac{2\kappa_{\mathrm{m}}}{\kappa_{\mathrm{m}}+\kappa_{\mathrm{p}}^{*}}A_{\mathrm{m}}R\cos\theta\right)^{2}d\theta. \tag{S35}$$

According to the minimum entropy production principle, $\phi\big(x(R)\big)=\pi/4$ should be satisfied. Equation (S35) takes the minimum value when

$$M\big(x(R)\big)\cos\Big(\phi\big(x(R)\big)\Big)=\frac{2\kappa_{\mathrm{m}}}{\kappa_{\mathrm{m}}+\kappa_{\mathrm{p}}^{*}}A_{\mathrm{m}}R. \tag{S36}$$

We reconsider the rotating particle, and the boundary conditions are

$$T_{\mathrm{m}}(r=R)=T_{\mathrm{p}}(r=R), \tag{S37}$$

$$-\kappa_{\mathrm{m}}\frac{\partial T_{\mathrm{m}}}{\partial r}(r=R)=-\kappa_{\mathrm{p}}\frac{\partial T_{\mathrm{p}}}{\partial r}(r=R). \tag{S38}$$

Substituting Eqs. (S24) and (S28) into Eq. (S38), we can derive

$$-\kappa_{\mathrm{m}}\left(A_{\mathrm{m}}-\frac{B_{\mathrm{m}}}{R^{2}}\right)\cos\theta=-\kappa_{\mathrm{p}}\sqrt{\frac{\Omega}{D}}M\big(x(R)\big)\cos\Big(\theta-\phi\big(x(R)\big)+\frac{\pi}{4}\Big). \tag{S39}$$

The substitution of Eqs. (S33) and (S36) into Eq. (S39) yields

$$-\kappa_{\mathrm{m}}\left(A_{\mathrm{m}}-\frac{\kappa_{\mathrm{m}}-\kappa_{\mathrm{p}}^{*}}{\kappa_{\mathrm{m}}+\kappa_{\mathrm{p}}^{*}}A_{\mathrm{m}}\right)=-\kappa_{\mathrm{p}}\sqrt{\frac{\Omega}{D}}\frac{2\kappa_{\mathrm{m}}}{\kappa_{\mathrm{m}}+\kappa_{\mathrm{p}}^{*}}A_{\mathrm{m}}R\frac{1}{\cos\Big(\phi\big(x(R)\big)\Big)}. \tag{S40}$$

Equation (40) can be reduced to

$$\kappa_{\mathrm{p}}^{*}=\kappa_{\mathrm{p}}\sqrt{\frac{2\Omega R^{2}}{D}}=\kappa_{\mathrm{p}}\sqrt{2\Phi}, \tag{S41}$$

where $\Phi=\Omega R^{2}D^{-1}$ plays a similar role to the Peclet number.

Supplementary Section 3: Effect of the thermal conductivity of the particles

We know from Eq. (S32) that with the increment of κ_{p}^{*}, the temperature gradient A_{p}^{*} in the particle decreases. Meanwhile, faster rotation enhances the effective thermal conductivity of the particles; see Eq. (S41).

Since rotation distorts the direction of isotherms in the particle, it also reduces the temperature gradient. We perform finite-element simulations based on a unit cell to quantify the effect. The temperature profiles with different rotation velocities are presented in Fig. S3*A*-*E*. The rotation direction affects the distortion direction of isotherms, and a larger rotation velocity leads to more sparse isotherms. The average longitudinal temperature gradient $\langle -T_{x}\rangle$ in the particle is an even function of Φ and is monotonically decreasing in the region $\Phi>0$ (Fig. S3*F*). Since the advantage of faster rotation is negated, the optimal rotation velocity exists for maximum thermal chirality.

Then we discuss the quantitative impact of the thermal conductivity of the particles on thermal chirality. When $\kappa_{\mathrm{p}}=0.2$ (Fig. S4*A*), the increment of κ_{xy} becomes slow, and the values of κ_{xx} with different R are not identical at $\Phi=0$. The maximum value of γ appears at the identical position of $\Phi\approx 21.4$. We further consider the thermal conductivity of the particles larger than that of the matrix, i.e., $\kappa_{\mathrm{p}}=5$ (Fig. S4*B*). The value of κ_{xy} quickly reaches a peak and then decreases, and the curves of κ_{xx} does not overlap. The peak of γ appears at the identical position of $\Phi \approx 4.2$, smaller than $\Phi \approx 21.4$ for $\kappa_{\mathrm{p}} = 0.2$. Finally, we keep the radius of the particles unchanged. With the increment of κ_{p}, the maximum value of γ and the corresponding value of Φ decrease (the arrow in Fig. S4*C*). For stronger thermal chirality (or larger γ), a smaller κ_{p} is better because it leads to a more significant temperature gradient in the rotating particles, enhancing the net transverse heat flux.

Supplementary Section 4: Size effect of the active thermal lattice

The size effect means effective thermal conductivity relies on the number of unit cells. We discuss three typical cases with $1 \times N$, $N \times 1$, and $N \times N$ unit cells (Fig. S5*A*). The effective thermal conductivities κ_{xy} and κ_{xx} are plotted as a function of the size N (Fig. S5*B*). For case I, the values of κ_{xy} and κ_{xx} are irrelevant to the size N, demonstrating no size effect. In contrast, the values of κ_{xy} and κ_{xx} show size dependence in case II, where κ_{xy} is decreasing and κ_{xx} is increasing. These two values finally approach constants because the active lattice becomes large enough. The variation ranges are about 1.26% for κ_{xy} and 0.54% for κ_{xx}, which are relatively small. Since the vertical stacking does not matter (case I), case III shows the same size effect as case II (Fig. S5*B*).

The size effect originates from translation symmetry breaking. The periodic lattice has natural structure translation symmetry, but the boundary conditions do not necessarily have translation symmetry. We focus on the temperature gradient on the boundary (Fig. S5*C*). For case I, the longitudinal temperature gradients $\partial_x T$ at different heights are the same due to the periodic boundary conditions at the upper and lower edges, so the translation symmetry of boundary conditions is maintained. The transverse stacking does not affect effective thermal conductivity. In contrast, for case II, the transverse temperature gradients $\partial_y T$ at the left and right boundaries differ from elsewhere due to their constant temperatures. The translation symmetry of boundary conditions is broken, so the size effect appears in case II. Translation symmetry breaking is crucially related to thermal chirality. If the particles do not rotate, thermal chirality disappears, and translation symmetry can be maintained.

We further present temperature profiles for intuitive understanding. The reference temperature profile with the Hall thermal conductivity is shown in Fig. S5*D*, demonstrating a uniform longitudinal temperature gradient. Figure S5*E* and *F* exhibits the temperature profile of an active thermal lattice with N taking 4 or 20. We also plot the temperature deviation profile $\delta = (T - T_{\mathrm{Ref}})/(T_{\mathrm{Hot}} - T_{\mathrm{Cold}})$ in Fig. S5*G* and *H*. With the increment of N, the longitudinal temperature gradient becomes more uniform. Translation symmetry breaking turns slight, so the size effect gradually vanishes (Fig. S5*B*).

Supplementary Section 5: Ideal properties of the experimental setup

We perform finite-element simulations based on the fabricated sample under the ideal condition without interfacial thermal resistance. The effective thermal conductivity and thermal chirality are presented in Fig. S6*A*. Since we use metals (i.e., copper and steel) with high thermal conductivities, the values of κ_{xy} and κ_{xx} are significantly enhanced, and they reach an unexpected order of magnitude 10^2 W m^{-1} K^{-1}. Nevertheless, thermal chirality does not strongly depend on specific materials. Due to the far smaller thermal conductivity of the particles than the matrix, thermal chirality is slightly enhanced and reaches a maximum value of $\gamma = 0.35$ when $R = 0.35$.

The temperature profiles with different Φ are presented in Fig. S6*B*. The upper and lower boundaries are thermally insulating, so heat flux is forbidden to flow out at the edges, leading to the slant of isotherms. Thermal chirality is intuitively reflected in the slant of isotherms. We also perform finite-element simulations based on the effective parameters calculated from periodic boundary conditions (Fig. S6*C*). Despite temperature fluctuations, the slant of isotherms agrees, proving the validity of our calculation method. The detailed temperature deviation profiles are presented in Fig. S6*D*.

Supplementary Section 6: Basic properties of anisotropic thermal chirality

Since there is no real-number solution to $\kappa'_{\mathrm{xy}} = \kappa'_{\mathrm{yx}} = 0$, an anisotropic Hall thermal conductivity tensor is rotation-varying and cannot be diagonalized; see Eqs. (S4)-(S7). For the second best, we expect $\overleftrightarrow{\kappa}'$ to be quasi-diagonalized, thus leading to two typical cases. The first case is $\kappa'_{\mathrm{xx}} = \kappa'_{\mathrm{yy}}$ and $\kappa'_{\mathrm{xy}} \neq \kappa'_{\mathrm{yx}}$, corresponding to Fig. 4*C* in the main text. Solving $\kappa'_{\mathrm{xx}} = \kappa'_{\mathrm{yy}}$, we obtain

$$\tan(2\theta_1) = \frac{\kappa_{\mathrm{xx}} - \kappa_{\mathrm{yy}}}{\kappa_{\mathrm{xy}} + \kappa_{\mathrm{yx}}}. \qquad [\mathrm{S42}]$$

The second case is $\kappa'_{\mathrm{xy}} = -\kappa'_{\mathrm{yx}}$ and $\kappa'_{\mathrm{xx}} \neq \kappa'_{\mathrm{yy}}$, corresponding to Fig. 4*E* in the main text. Solving $\kappa'_{\mathrm{xy}} = -\kappa'_{\mathrm{yx}}$, we derive

$$\tan(2\theta_2) = -\frac{\kappa_{\mathrm{xy}} + \kappa_{\mathrm{yx}}}{\kappa_{\mathrm{xx}} - \kappa_{\mathrm{yy}}}. \qquad [\mathrm{S43}]$$

With the rotation angle taking θ_1 or θ_2, a general thermal conductivity tensor can be quasi-diagonalized. Due to $\tan(2\theta_1)\tan(2\theta_2) = -1$, we also derive $\theta_1 = \theta_2 + \pm\pi/4$, agreeing with the results in Fig. 4*C* and *E* in the main text.

The anisotropic feature makes thermal chirality depend on direction. We can still characterize thermal chirality by the transverse to longitudinal heat flux ratio. According to Eqs. (S4)-(S7), we can express thermal chirality γ as

$$\gamma = \frac{J_{\mathrm{y}}}{J_{\mathrm{x}}} = \frac{\kappa'_{\mathrm{xy}}}{\kappa'_{\mathrm{xx}}} = \frac{\kappa_{\mathrm{xy}}\cos^2\theta_0 - \kappa_{\mathrm{yx}}\sin^2\theta_0 + (\kappa_{\mathrm{xx}} - \kappa_{\mathrm{yy}})\cos\theta_0\sin\theta_0}{\kappa_{\mathrm{xx}}\cos^2\theta_0 + \kappa_{\mathrm{yy}}\sin^2\theta_0 - (\kappa_{\mathrm{xy}} + \kappa_{\mathrm{yx}})\cos\theta_0\sin\theta_0}. \qquad [\mathrm{S44}]$$

If we start with a quasi-diagonalized case with $\kappa_{\mathrm{xx}} = \kappa_{\mathrm{yy}}$, anisotropic thermal chirality described by Eq. (S44) can be reduced to

$$\gamma = \frac{\kappa_{\mathrm{xy}}\cos^2\theta_0 - \kappa_{\mathrm{yx}}\sin^2\theta_0}{\kappa_{\mathrm{xx}} - (\kappa_{\mathrm{xy}} + \kappa_{\mathrm{yx}})\cos\theta_0\sin\theta_0}. \qquad [\mathrm{S45}]$$

When $\kappa_{\mathrm{xy}} = -\kappa_{\mathrm{yx}}$, thermal chirality is further simplified as $\gamma = \kappa_{\mathrm{xy}}/\kappa_{\mathrm{xx}}$, which features rotation invariance and demonstrates no anisotropy.

By rotating a specific angle, we can construct an anisotropic Hall thermal conductivity from a quasi-diagonalized thermal conductivity. The two types of quasi-diagonalized thermal conductivities are designed with practical structures in Fig. 4 in the main text. The thermal conductivity of the matrix is diagonalizable with components of κ_{mx} and κ_{my}. The effective thermal conductivity of the active thermal lattice has the form of Eq. (S1). To obtain these four values from finite-element simulations (i.e., κ_{xx}, κ_{yy}, κ_{xy}, and κ_{yx}), we first apply a longitudinal temperature gradient by setting the left and right boundaries with constant temperatures. The upper and lower boundaries are periodic. Then we obtain

$$\kappa_{\mathrm{xx}} = \frac{J_{\mathrm{x}}}{G}, \qquad [\mathrm{S46}]$$

$$\kappa_{\mathrm{xy}} = \frac{J_{\mathrm{y}}}{G}, \qquad [\mathrm{S47}]$$

where J_{x} and J_{y} are the longitudinal and transverse heat fluxes, and G is the negative temperature gradient. We also use a transverse temperature gradient by setting the upper and lower boundaries with constant temperatures, and the left and right boundaries become periodic. Then we derive

$$\kappa_{\mathrm{yy}} = \frac{J_{\mathrm{y}}}{G}, \qquad [\mathrm{S48}]$$

$$\kappa_{\mathrm{yx}} = \frac{J_{\mathrm{x}}}{G}. \qquad [\mathrm{S49}]$$

The effective thermal conductivity with different matrices is presented in Fig. S7. With a more anisotropic thermal conductivity of the matrix, $\kappa_{\mathrm{xx}} = \kappa_{\mathrm{yy}}$ is kept when $\alpha = \pi/4$ (Fig. S7*A* and *C*), but $\kappa_{\mathrm{xy}} = -\kappa_{\mathrm{yx}}$ is deviated when $\alpha = 0$. Stronger anisotropy yields a larger deviation (Fig. S7*B* and *D*).

The size effect becomes apparent when it comes to anisotropy. The thermal conductivity of the matrix is first set as $\mathrm{diag}[0.5, 2]$ with the vertical thermal conductivity higher than the horizontal one (Fig. S8*A*). The value of κ_{xy} is almost invariant with the increment of N, but the value of $-\kappa_{\mathrm{yx}}$

decreases. The value of κ_{xx} is also invariant with the increment of N, and the value of κ_{yy} increases. This phenomenon results from the larger κ_{my} than κ_{mx}. When we apply a horizontal thermal field, a larger κ_{my} tends to keep the isotherms vertically straight. Hence, the size effect is almost absent for κ_{xy} and κ_{xx}. We also consider the temperature deviation δ between a practical structure and an ideal parameter. The global average temperature deviation $\langle|\delta|\rangle$ is a reliable physical quantity to reflect the difference. With the increment of N, the value of $\langle|\delta|\rangle$ decreases, indicating that the practical structure becomes homogeneous. We plot the case of $N = 10$ in the insets. With the enhancement of the anisotropy degree, the size effect becomes more crucial, especially for the values of $-\kappa_{\mathrm{yx}}$ and κ_{yy} (Fig. S8*B* and *C*).

The size effect is related to the translation symmetry breaking of boundary conditions. On the one hand, anisotropy yields significant translation symmetry breaking. On the other hand, as the whole system becomes more homogeneous (with a larger N), translation symmetry breaking turns weaker. Thus, effective thermal conductivity finally becomes constant with the increment of N.

Supplementary Section 7: Linking thermal chirality and transformation thermotics

The transformation theory or transformation thermotics (5-8) still applies to Hall thermal conductivity. The transformed thermal conductivity is chiral and anisotropic. That is why we discuss the approach to anisotropic thermal chirality. For a coordinate transformation determined by the Jacobian matrix A, the transformed thermal conductivity $\overleftrightarrow{\kappa}'$ is

$$\overleftrightarrow{\kappa}' = \frac{A\overleftrightarrow{\kappa}A^{\dagger}}{\det A}. \qquad [\mathrm{S50}]$$

Since $\overleftrightarrow{\kappa}$ is a Hall thermal conductivity, $\overleftrightarrow{\kappa}'$ is generally chiral, anisotropic, and inhomogeneous.

We take Hall thermal cloaking, concentrating, and rotating as three typical examples of the calculation process. Coordinate transformations are usually written in cylindrical coordinates. We need to express the original isotropic Hall thermal conductivity from the Cartesian coordinates (x, y) to cylindrical coordinates (r, θ). The expression of the original isotropic Hall thermal conductivity $\overleftrightarrow{\kappa}$ in the Cartesian coordinates (also denoted as $\overleftrightarrow{\kappa}_{\mathrm{Car}}$ for clarity) is

$$\overleftrightarrow{\kappa}_{\mathrm{Car}} = \begin{bmatrix} \kappa_{\mathrm{xx}} & \kappa_{\mathrm{yx}} \\ \kappa_{\mathrm{xy}} & \kappa_{\mathrm{yy}} \end{bmatrix}. \qquad [\mathrm{S51}]$$

Its expression in the cylindrical coordinates (denoted as $\overleftrightarrow{\kappa}_{\mathrm{cyl}}$) is

$$\overleftrightarrow{\kappa}_{\mathrm{cyl}} = \begin{bmatrix} \kappa_{\mathrm{rr}} & \kappa_{\theta\mathrm{r}} \\ \kappa_{\mathrm{r}\theta} & \kappa_{\theta\theta} \end{bmatrix}, \qquad [\mathrm{S52}]$$

where the components can be expressed as

$$\kappa_{\mathrm{rr}} = \kappa_{\mathrm{xx}} \cos^2\theta + \kappa_{\mathrm{yy}} \sin^2\theta - \left(\kappa_{\mathrm{xy}} + \kappa_{\mathrm{yx}}\right) \cos\theta \sin\theta, \qquad [\mathrm{S53}]$$

$$\kappa_{\theta\theta} = \kappa_{\mathrm{yy}} \cos^2\theta + \kappa_{\mathrm{xx}} \sin^2\theta + \left(\kappa_{\mathrm{xy}} + \kappa_{\mathrm{yx}}\right) \cos\theta \sin\theta, \qquad [\mathrm{S54}]$$

$$\kappa_{\mathrm{r}\theta} = \kappa_{\mathrm{xy}} \cos^2\theta - \kappa_{\mathrm{yx}} \sin^2\theta + \left(\kappa_{\mathrm{xx}} - \kappa_{\mathrm{yy}}\right) \cos\theta \sin\theta, \qquad [\mathrm{S55}]$$

$$\kappa_{\theta\mathrm{r}} = \kappa_{\mathrm{yx}} \cos^2\theta - \kappa_{\mathrm{xy}} \sin^2\theta + \left(\kappa_{\mathrm{xx}} - \kappa_{\mathrm{yy}}\right) \cos\theta \sin\theta. \qquad [\mathrm{S56}]$$

An isotropic case features $\kappa_{\mathrm{xx}} = \kappa_{\mathrm{yy}}$ and $\kappa_{\mathrm{xy}} = -\kappa_{\mathrm{yx}}$, so Eqs. (S53)-(S56) become

$$\kappa_{\mathrm{rr}} = \kappa_{\mathrm{xx}}, \qquad [\mathrm{S57}]$$

$$\kappa_{\theta\theta} = \kappa_{\mathrm{yy}}, \qquad [\mathrm{S58}]$$

$$\kappa_{\mathrm{r}\theta} = \kappa_{\mathrm{xy}}, \qquad [\mathrm{S59}]$$

$$\kappa_{\theta\mathrm{r}} = \kappa_{\mathrm{yx}}. \qquad [\mathrm{S60}]$$

For an isotropic Hall thermal conductivity, its expression in cylindrical coordinates is the same as in the Cartesian coordinates.

Then we consider the coordinate transformation for thermal cloaking,

$$r' = ar + b \ (0 \le r \le R_2), \qquad [\mathrm{S61}]$$

$$\theta' = \theta \ (0 \le r \le R_2), \qquad [\mathrm{S62}]$$

with $a = (R_2 - R_1)/R_2$ and $b = R_1$. R_1 and R_2 are the inner and outer radii of the cloak. (r', θ') are the coordinates in physical space, and (r, θ) are the coordinates in virtual space. The transformation turns a solid circle into a hollow ring. The corresponding Jacobian transformation matrix is

$$A=\begin{bmatrix}\frac{\partial r'}{\partial r} & \frac{\partial r'}{r\partial\theta}\\ \frac{r'\partial\theta'}{\partial r} & \frac{r'\partial\theta'}{r\partial\theta}\end{bmatrix}=\begin{bmatrix}a & 0\\ 0 & \frac{ar'}{r'-b}\end{bmatrix}. \quad [S63]$$

Then the transformed thermal conductivity is

$$\overleftrightarrow{\kappa}'=\frac{A\overleftrightarrow{\kappa}A^{\dagger}}{\det A}=\begin{bmatrix}\frac{r'-b}{r'}\kappa_{\mathrm{xx}} & \kappa_{\mathrm{yx}}\\ \kappa_{\mathrm{xy}} & \frac{r'}{r'-b}\kappa_{\mathrm{yy}}\end{bmatrix}. \quad [S64]$$

Compared with a familiar thermal cloak, the thermal conductivity of Hall thermal cloaking has two nonzero off-diagonal components being opposite constants.

Thermal concentrating first compresses a solid circle with a radius of R_{m} into a smaller one with a radius of R_1. Then the hollow ring with inner and outer radii of R_{m} and R_2 is stretched into a bigger one with inner and outer radii of R_1 and R_2. The corresponding coordinate transformation is

$$r'=cr\ (0\le r<R_{\mathrm{m}}), \quad [S65]$$

$$r'=dr+f\ (R_{\mathrm{m}}\le r\le R_2), \quad [S66]$$

$$\theta'=\theta\ (0\le r\le R_2), \quad [S67]$$

with $c=R_1/R_{\mathrm{m}}$, $d=(R_2-R_1)/(R_2-R_{\mathrm{m}})$, and $f=R_2(R_1-R_{\mathrm{m}})/(R_2-R_{\mathrm{m}})$. The Jacobian transformation matrix in the core is $A=cI$, with I being the second-order unit matrix. The Jacobian transformation matrix in the shell is

$$A=\begin{bmatrix}d & 0\\ 0 & \frac{dr'}{r'-f}\end{bmatrix}. \quad [S68]$$

The thermal conductivity of the core is invariant after transformation, and that of the concentrator becomes

$$\overleftrightarrow{\kappa}'=\begin{bmatrix}\frac{r'-f}{r'}\kappa_{\mathrm{xx}} & \kappa_{\mathrm{yx}}\\ \kappa_{\mathrm{xy}} & \frac{r'}{r'-f}\kappa_{\mathrm{yy}}\end{bmatrix}. \quad [S69]$$

The coordinate transformation for thermal rotating is

$$r'=r\ (0\le r\le R_2), \quad [S70]$$

$$\theta'=\theta+\varphi\ (0\le r<R_1), \quad [S71]$$

$$\theta'=\theta+\frac{(R_2-r)\varphi}{R_2-R_1}\ (R_1\le r\le R_2), \quad [S72]$$

where φ is the anticlockwise rotation angle. The Jacobian transformation matrix in the core is $A=I$, making the thermal conductivity of the core invariant after transformation. The Jacobian transformation matrix in the shell is

$$A=\begin{bmatrix}1 & 0\\ -\frac{r'\varphi}{R_2-R_1} & 1\end{bmatrix}. \quad [S73]$$

The corresponding thermal conductivity of the rotator is

$$\overleftrightarrow{\kappa}'=\begin{bmatrix}\kappa_{\mathrm{xx}} & -\frac{r'\varphi}{R_2-R_1}\kappa_{\mathrm{xx}}+\kappa_{\mathrm{yx}}\\ -\frac{r'\varphi}{R_2-R_1}\kappa_{\mathrm{xx}}+\kappa_{\mathrm{xy}} & \left(\frac{r'\varphi}{R_2-R_1}\right)^2\kappa_{\mathrm{xx}}+\kappa_{\mathrm{yy}}\end{bmatrix}. \quad [S74]$$

The simulation results are shown in Fig. S9. The temperature gradient is uniform when a uniform Hall thermal conductivity meets the periodic boundary conditions (Fig. S9*A*). Then we put a particle with opposite thermal chirality in the matrix. The interface effect induced by opposite thermal chirality distorts the temperature profile (Fig. S9*B*), making the object thermally visible. We design a conventional thermal cloak to remove the temperature distortion, but it fails (Fig. S9*C*) because a Hall parameter inevitably has the interface effect with a common parameter. The temperature distortion is removed (Fig. S9*D*) when we design a Hall thermal cloak with an anisotropic Hall thermal conductivity described by Eq. (S64). Since the temperature profile in the background recovers, the object cannot be thermally detected, achieving the cloaking effect.

Similarly, we demonstrate Hall concentrating (Fig. S9*E*) and rotating (Fig. S9*F*) functions, indicating that the density and direction of isotherms can be flexibly regulated. The insulating boundary conditions further replace the periodic boundary conditions, and the corresponding results are still satisfying (Fig. S9*G*-*L*). The main difference between the two boundary conditions lies in the reference temperature profiles (Fig. S9*A* and *G*).

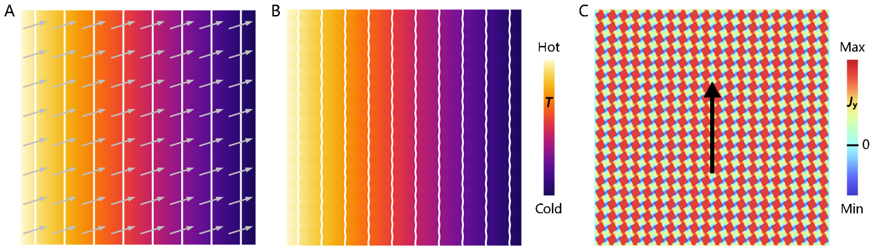

Fig. S1. Basic properties of thermal chirality. (*A*) Temperature profile of a Hall thermal conductivity with $\kappa_{\mathrm{xy}} = -\kappa_{\mathrm{yx}} = 0.4$ and $\kappa_{\mathrm{xx}} = \kappa_{\mathrm{yy}} = 1.3$ W m^{-1} K^{-1}. (*B*) Temperature profile of an active lattice composed of 20×20 unit cells. (*C*) Transverse heat flux profile with upward net heat flux. The transverse heat flux in the particles is averaged.

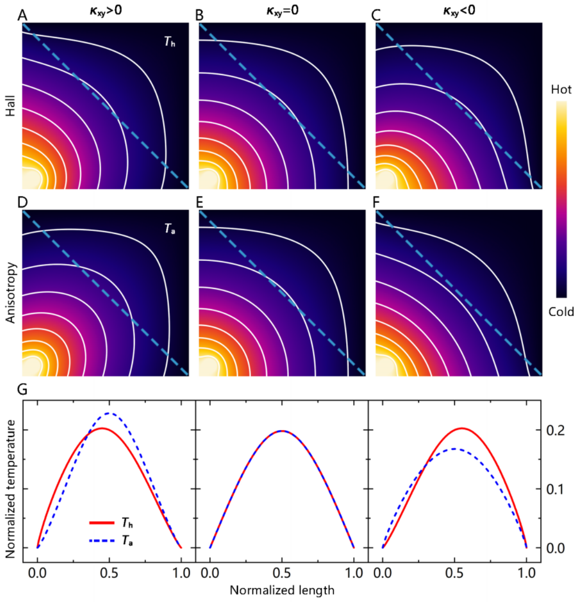

Fig. S2. Comparison between Hall and anisotropic thermal conductivities whose diagonal components are $\kappa_{\mathrm{xx}} = \kappa_{\mathrm{yy}} = 1.3$ W m^{-1} K^{-1}. $\kappa_{\mathrm{xy}} = -\kappa_{\mathrm{yx}}$ for the Hall case and $\kappa_{\mathrm{xy}} = \kappa_{\mathrm{yx}}$ for the anisotropic case. (*A* and *D*) $\kappa_{\mathrm{xy}} = 0.4$ W m^{-1} K^{-1}. (*C* and *F*) $\kappa_{\mathrm{xy}} = -0.4$ W m^{-1} K^{-1}. The left and bottom boundaries are insulating. The upper and right boundaries have a constant low temperature. A constant high temperature appears at the left-bottom corner. (*G*) Temperature distributions on the dashed lines.

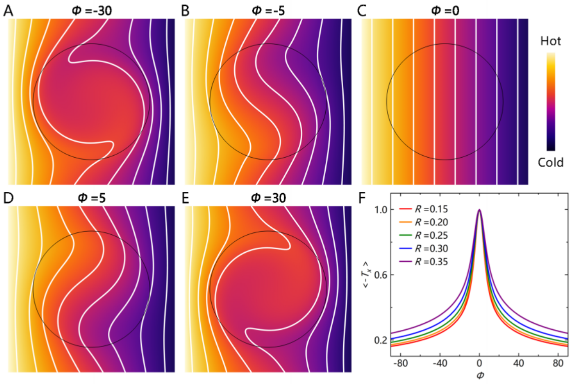

Fig. S3. Rotation influences on temperature profiles. (*A*-*E*) Temperature profiles with $R = 0.35$, $\kappa_\mathrm{m}/\kappa_\mathrm{p} = 1$, and different Φ. The external temperature gradient is 1. The upper and lower boundaries are periodic. (*F*) Average longitudinal temperature gradient $\langle -T_x \rangle$ in the particle as a function of Φ with different R.

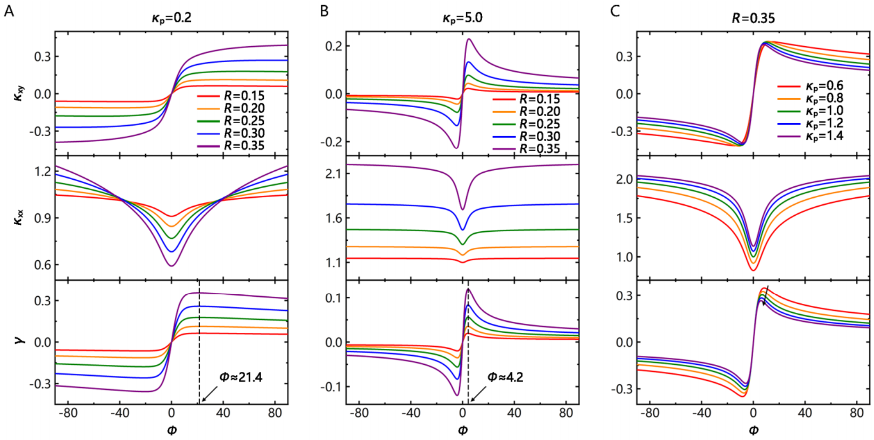

Fig. S4. Effect of the thermal conductivity of the particle. (*A*-*C*) Effective thermal conductivity of an active lattice with 20×20 unit cells as a function of the dimensionless parameter $\Phi = \Omega R^2 D_{\mathrm{p}}^{-1}$. The thermal conductivity of the matrix is $\kappa_{\mathrm{m}} = 1$, and that of the particles is (*A*) $\kappa_{\mathrm{p}} = 0.2$ and (*B*) $\kappa_{\mathrm{p}} = 5$. (*C*) The radius of the particles is $R = 0.35$. The unit of thermal conductivity is 1 W m^{-1} K^{-1}.

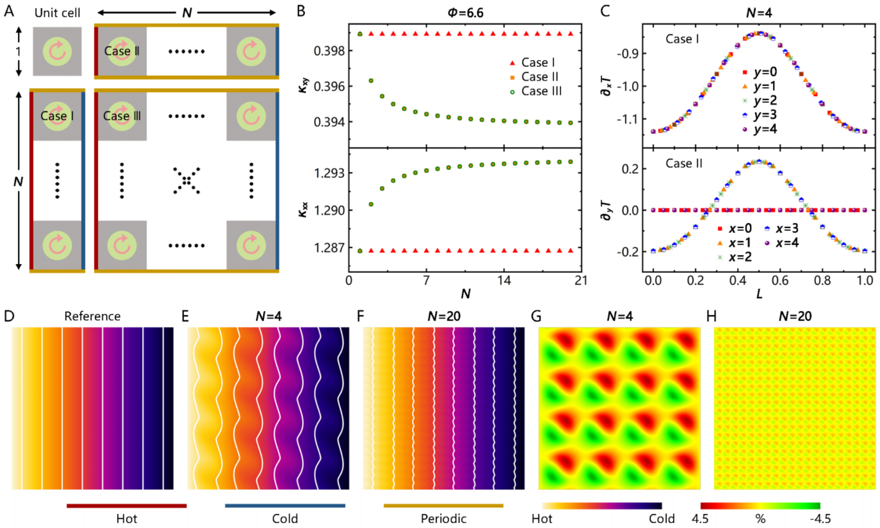

Fig. S5. Size effect of the active thermal lattice. (*A*) Three typical cases. (*B*) Effective thermal conductivity as a function of the size N with $\kappa_\mathrm{m}/\kappa_\mathrm{p} = 1$, $R = 0.35$, and $\Phi = 6.6$. (*C*) Temperature gradient distributions with $N = 4$. (*D*) Reference temperature profile T_Ref of a Hall thermal conductivity with $\kappa_\mathrm{xy} = 0.4$ and $\kappa_\mathrm{xx} = 1.3$ W m^{-1} K^{-1}. (*E* and *F*) Temperature profiles T of the active thermal lattices with $N = 4$ and $N = 20$ (scaled to the same size). (*G* and *H*) Temperature deviation profiles $\delta = (T - T_\mathrm{Ref})/(T_\mathrm{Hot} - T_\mathrm{Cold})$.

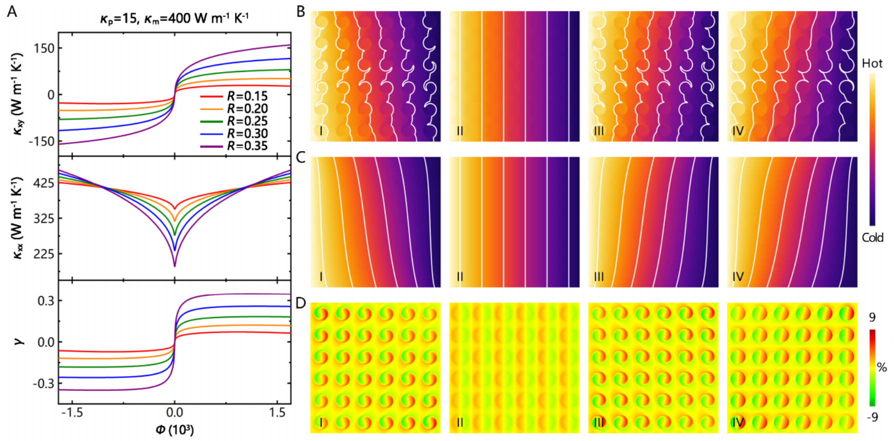

Fig. S6. Simulations of the experimental setup without interfacial thermal resistance. (*A*) Effective thermal conductivity of the fabricated sample with 6×6 unit cells as a function of the dimensionless parameter $\Phi = \Omega R^2 D_\mathrm{p}^{-1}$. The matrix is copper with thermal conductivity of 400 W m^{-1} K^{-1}, mass density of 8900 kg m^{-3}, and heat capacity of 390 J kg^{-1} K^{-1}. The particles are steel with thermal conductivity of 15 W m^{-1} K^{-1}, mass density of 7930 kg m^{-3}, and heat capacity of 500 J kg^{-1} K^{-1}. (*B*) Temperature profiles with the area fraction of the particles being 0.38. From I to IV, Φ takes -100, 0, 100, and 1000, respectively. (*C*) Temperature profiles of corresponding ideal Hall thermal conductivities shown in (*A*). (*D*) Temperature deviation profiles between (*B*) and (*C*).

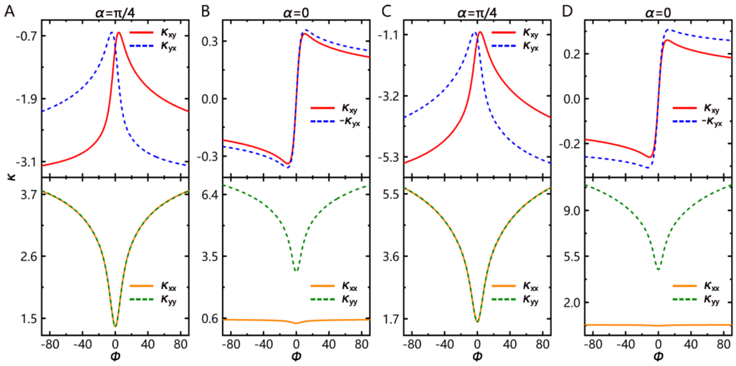

Fig. S7. Influences of the matrix with more anisotropic thermal conductivities. (*A*-*D*) Effective thermal conductivity of an active lattice with 20×20 unit cells as a function of the dimensionless parameter $\Phi = \Omega R^2 D_\mathrm{p}^{-1}$ with $\kappa_\mathrm{p} = 1$ and $R = 0.35$. The anisotropic thermal conductivity of the matrix is (*A* and *B*) $\overleftrightarrow{\kappa}_\mathrm{m} = \mathrm{diag}[0.2, 5]$ and (*C* and *D*) $\overleftrightarrow{\kappa}_\mathrm{m} = \mathrm{diag}[0.1, 10]$. The unit of thermal conductivity is 1 W m^{-1} K^{-1}.

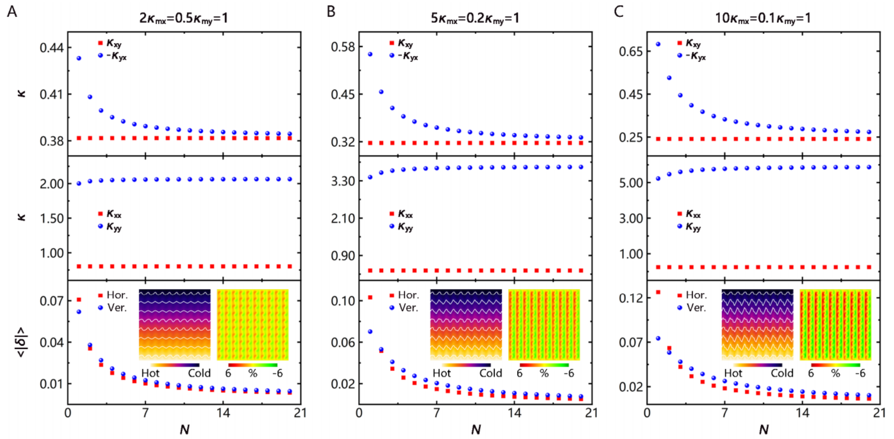

Fig. S8. Size effect of the anisotropic thermal lattice. Effective thermal conductivity and average temperature deviation $\langle|\delta|\rangle$ as a function of the size N with $\kappa_\mathrm{p} = 1$, $R = 0.35$, and $\Phi = 6.6$. (*A*) $\overleftrightarrow{\kappa}_\mathrm{m} = \mathrm{diag}[0.5, 2]$. (*B*) $\overleftrightarrow{\kappa}_\mathrm{m} = \mathrm{diag}[0.2, 5]$. (*C*) $\overleftrightarrow{\kappa}_\mathrm{m} = \mathrm{diag}[0.1, 10]$. The insets in the last rows are the temperature and deviation profiles with $N = 10$ in a transverse temperature gradient. The unit of thermal conductivity is 1 W m^{-1} K^{-1}.

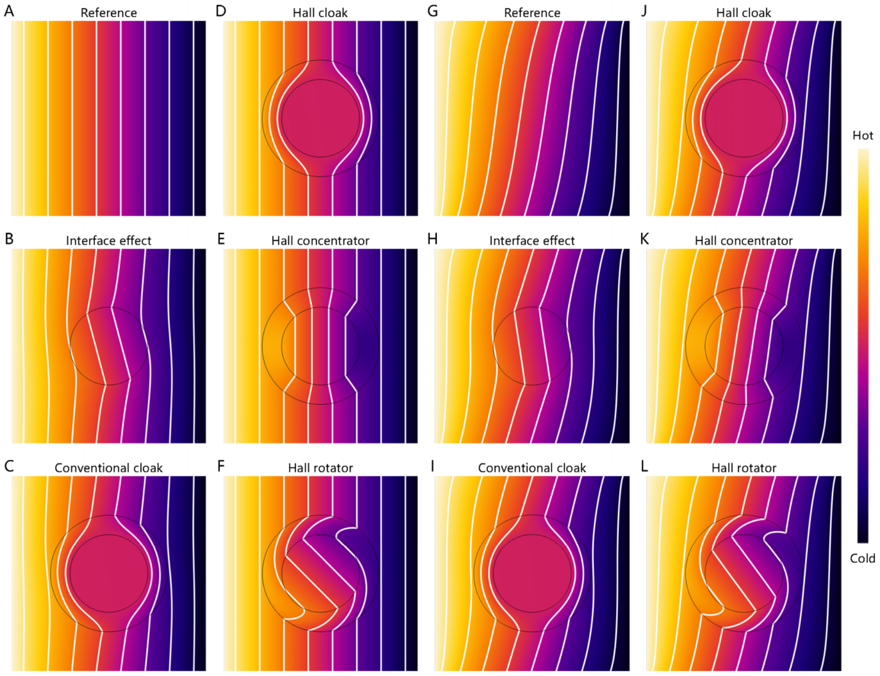

Fig. S9. Applications of anisotropic thermal chirality. Three typical functions with (*A*-*F*) periodic and (*G*-*L*) insulating boundary conditions at the upper and lower edges. (*A*) Reference temperature profile with $\gamma = 4/13$. (*B*) Interface effect induced by a particle with $\gamma = -4/13$ (opposite thermal chirality compared to the background). (*C*) Conventional cloak. (*D*) Hall cloak. (*E*) Hall concentrator. (*F*) Hall rotator. (*G*-*L*) Same as (*A*-*F*) with insulating boundary conditions replacing periodic boundary conditions at the upper and lower boundaries.

SI References

1. Y. Li, K.-J. Zhu, Y.-G. Peng, W. Li, T. Yang, H.-X. Xu, H. Chen, X.-F. Zhu, S. Fan, C.-W. Qiu, Thermal meta-device in analogue of zero-index photonics. *Nat. Mater.* **18**, 48-54 (2019).
2. G. Xu, K. Dong, Y. Li, H. Li, K. Liu, L. Li, J. Wu, C.-W. Qiu, Tunable analog thermal material. *Nat. Commun.* **11**, 6028 (2020).
3. J. Li, Y. Li, P.-C. Cao, T. Yang, X.-F. Zhu, W. Wang, C.-W. Qiu, A continuously tunable solid-like convective thermal metadevice on the reciprocal line. *Adv. Mater.* **32**, 2003823 (2020).
4. G. W. Milton, *The Theory of Composites* (Cambridge University Press, Cambridge, 2002).
5. S. Yang, J. Wang, G. Dai, F. Yang, J. Huang, Controlling macroscopic heat transfer with thermal metamaterials: Theory, experiment and application. *Phys. Rep.* **908**, 1-65 (2021).
6. Z. Zhang, L. Xu, T. Qu, M. Lei, Z.-K. Lin, X. Ouyang, J.-H. Jiang, J. Huang, Diffusion metamaterials. *Nat. Rev. Phys.* **5**, 218-235 (2023).
7. Y. Li, W. Li, T. Han, X. Zheng, J. Li, B. Li, S. Fan, C.-W. Qiu, Transforming heat transfer with thermal metamaterials and devices. *Nat. Rev. Mater.* **6**, 488-507 (2021).
8. W.-S. Yeung, R.-J. Yang, *Introduction to Thermal Cloaking: Theory and Analysis in Conduction and Convection* (Springer, Singapore, 2022).